Naval Research Laboratory

Stennis Space Center, MS 39529-5004

NRL/MR/7320--16-9649

Implementation of a Balance Operator in NCOM

MAX YAREMCHUK
PAUL J. MARTIN

Ocean Dynamics and Prediction Branch
Oceanography Division

April 7, 2016

REPORT DOCUMENTATION PAGE

Form Approved
OMB No. 0704-0188

1. REPORT DATE *(DD-MM-YYYY)*
07-04-2016

2. REPORT TYPE
Memorandum Report

3. DATES COVERED *(From - To)*

4. TITLE AND SUBTITLE

Implementation of a Balance Operator in NCOM

5a. CONTRACT NUMBER

5b. GRANT NUMBER

5c. PROGRAM ELEMENT NUMBER
061153N

6. AUTHOR(S)

Max Yaremchuk and Paul J. Martin

5d. PROJECT NUMBER

5e. TASK NUMBER

5f. WORK UNIT NUMBER
73-4874-06-5

7. PERFORMING ORGANIZATION NAME(S) AND ADDRESS(ES)

Naval Research Laboratory
Oceanography Division
Stennis Space Center, MS 39529-5004

8. PERFORMING ORGANIZATION REPORT NUMBER

NRL/MR/7320--16-9649

9. SPONSORING / MONITORING AGENCY NAME(S) AND ADDRESS(ES)

Office of Naval Research
One Liberty Center
875 North Randolph Street, Suite 1425
Arlington, VA 22203-1995

10. SPONSOR / MONITOR'S ACRONYM(S)

ONR

11. SPONSOR / MONITOR'S REPORT NUMBER(S)

12. DISTRIBUTION / AVAILABILITY STATEMENT

Approved for public release; distribution is unlimited.

13. SUPPLEMENTARY NOTES

14. ABSTRACT

The balance operator and its adjoint for the Navy Coastal Ocean Model (NCOM) have been coded. The operator is implemented in two modes: (a) with and (b) without the integral continuity constraint. Testing the code in an Adriatic Sea configuration has shown that although the a-mode option is several times more computationally expensive, it provides half the ageostrophic motions excited by perturbations with a typical horizontal scale of the internal Rossby radius of deformation. For a state vector of 1.5M degrees of freedom, the total CPU time required by the code is negligible compared to the CPU time required by 1 hour of NCOM integration (i.e., 15 and 80 times less for the a- and b-mode options, respectively). The code could be used in the design of the background error covariance operators in both variational and ensemble applications of data assimilation.

15. SUBJECT TERMS

Balance operator
Background error covariance
Data assimilation
Ocean modeling

16. SECURITY CLASSIFICATION OF:			**17. LIMITATION OF ABSTRACT**	**18. NUMBER OF PAGES**	**19a. NAME OF RESPONSIBLE PERSON**
a. REPORT	**b. ABSTRACT**	**c. THIS PAGE**			Max Yaremchuk
Unclassified Unlimited	Unclassified Unlimited	Unclassified Unlimited	Unclassified Unlimited	16	**19b. TELEPHONE NUMBER** *(include area code)* (228) 688-5259

Standard Form 298 (Rev. 8-98)
Prescribed by ANSI Std. Z39.18

CONTENTS

IMPLEMENTATION OF A BALANCE OPERATOR IN NCOM

1. INTRODUCTION

1.1 Balance Constraints

Due to the sparsity of oceanographic observations, a common practice in oceanic data assimilation is to constrain the model state increments to be in (approximate) geostrophic and hydrostatic balance. This strategy allows one to extract the most persistent modes of variability from the data and filter out smaller/faster scale motions that are barely resolved by the observations. The geostrophic and hydrostatic balance constraints are supplemented by the (linearized) equation of state and, quite often, by additional, linear relationships between temperature and salinity ($T-S$ constraints), and/or an integral continuity constraint.

The basics of the above mentioned "balance operator technique" were originally developed for meteorological data assimilation (Derber and Bouttier 1999; Cullen 2003) and later implemented in oceanographic applications of variational data assimilation (Weaver et al. 2005).

To ensure computational efficiency, the balance constraints are introduced as a sequence of linear operations on the "unbalanced" (statistically independent) components of the ocean state $\mathbf{x}_1 = [T(\boldsymbol{x}, z), S(\boldsymbol{x}, z)]$, which produces the balanced constituents of the remaining part of the state vector $\mathbf{x}_2 = [\vec{\boldsymbol{u}}(\boldsymbol{x}, z), \zeta(\boldsymbol{x})]$. After that, the unbalanced constituents $\tilde{\mathbf{x}}_2$ of $\mathbf{x}_2$ are added to obtain the full update of the ocean state vector. To be more specific, assume that the model state variables $\{T, S, \zeta, \vec{\boldsymbol{u}}\}$ are represented by the M-dimensional vector $\mathbf{y} \in \mathcal{R}^M$ of the model fields' values at the computational grid points. The balance constraints are introduced by partitioning $\mathbf{y}$ as follows (Weaver et al. 2005):

$$\mathbf{y} = \begin{bmatrix} \mathbf{x}_1 \\ \mathbf{x}_2 \end{bmatrix}, \quad \mathbf{x}_1 = \begin{bmatrix} T \\ S \end{bmatrix} \in \mathcal{R}^{M_1}, \quad \mathbf{x}_2 = \begin{bmatrix} \vec{\boldsymbol{u}} \\ \zeta \end{bmatrix} \in \mathcal{R}^{M_2}, \quad M_1 + M_2 = M, \tag{1}$$

and representing $\mathbf{x}_2$ in the form $\mathbf{x}_2 = \mathbf{L}\mathbf{x}_1 + \tilde{\mathbf{x}}_2$, where $\mathbf{L}$ stands for the balance operator and $\tilde{\mathbf{x}}_2$ denotes the unbalanced constituents of $\mathbf{x}_2$. The discretized version of the operator $\mathbf{L}$ can be symbolically represented by an $M_1 \times M_2$ matrix

$$\begin{bmatrix} \vec{\boldsymbol{u}} \\ \zeta \end{bmatrix} = \begin{bmatrix} \mathsf{eq.of\quad state} \\ \mathsf{geostrophy} \\ \mathsf{hydrostatics} \\ \mathsf{continuity} \end{bmatrix} \begin{bmatrix} T \\ S \end{bmatrix}, \tag{2}$$

which is a finite-difference discretization of the following constraints (in the sequence they are symbolically written above):

Manuscript approved September 11, 2015.

$$\rho = \rho_0 + \alpha(\boldsymbol{x}, z)T + \beta(\boldsymbol{x}, z)S, \tag{3}$$

$$\vec{\boldsymbol{u}} = \frac{1}{f(\boldsymbol{x})\rho_0}\boldsymbol{k} \times \nabla p, \tag{4}$$

$$\partial_z p = -g\rho, \qquad p(\boldsymbol{x}, 0) = \rho_0 g\zeta(\boldsymbol{x}), \tag{5}$$

$$0 = \mathrm{div} \int\limits_{h(\boldsymbol{x})}^{0} \vec{\boldsymbol{u}} dz, \tag{6}$$

where $\boldsymbol{x} = (x, y)$ is the horizontal coordinate, z is the vertical coordinate, ρ_0 is the mean density of seawater, α and β are the Taylor expansion coefficients in the linearized equation of state (which depend on the spatial coordinates because the background temperature T_b and salinity S_b fields do), f is the Coriolis parameter, $\boldsymbol{k}$ is the vertical unit vector, ∇ is the horizontal gradient, p is the pressure, h is the ocean depth, and g is the gravitational acceleration. In applications, these constraints are usually modified to form the following sequence of operations which linearly map the input $\mathbf{x}_1 = [T, S]$ to the output $\mathbf{x}_2 = [\vec{\boldsymbol{u}}, \zeta]$:

$$\rho = \rho_0 + \alpha(\boldsymbol{x}, z)T + \beta(\boldsymbol{x}, z)S, \tag{7}$$

$$\nabla h(\boldsymbol{x})\nabla\zeta = \mathrm{div} \int\limits_{h(\boldsymbol{x})}^{0} \int\limits_{z}^{0} \nabla\rho(\boldsymbol{x}, z')dz'dz, \tag{8}$$

$$p = g\left[\rho_0\zeta(\boldsymbol{x}) + \int\limits_{z}^{0} \rho(\boldsymbol{x}, z')dz'\right], \tag{9}$$

$$\vec{\boldsymbol{u}} = \frac{1}{f(\boldsymbol{x})\rho_0}\boldsymbol{k} \times \nabla p.. \tag{10}$$

The equation (8) involves an iterative inversion of the elliptic operator $\nabla h\nabla$, which increases the computational cost of $\mathbf{L}$. For that reason, the respective constraint (integral continuity) is sometimes replaced by assigning "a level of no motion" (setting $p = 0$) at a certain reference depth z_{ref}, or at the bottom:

$$\zeta = -\frac{1}{\rho_0} \int\limits_{h}^{0} \rho(\boldsymbol{x}, z)dz. \tag{11}$$

A more general version of $\mathbf{L}$ is obtained by splitting the salinity field perturbations S into balanced $\overline{S}$ and unbalanced $\tilde{S}$ components:

$$S \to \overline{S} + \tilde{S} = \theta(\boldsymbol{x}, z)T + \tilde{S}, \tag{12}$$

where θ is the user-supplied scalar field describing the spatial variability of the $T - S$ relationship.

Since the balanced and unbalanced components are assumed to be uncorrelated, it is desirable to preserve the total salinity error variance estimated from the previous analyses. In the presented formulation of the balance operator, this constraint is introduced by the user-defined coefficient $\gamma(\boldsymbol{x}, z)$:

$$S = \gamma\overline{S} + \sqrt{1 - \gamma^2}\tilde{S} = \gamma\theta T + \sqrt{1 - \gamma^2}\tilde{S}. \tag{13}$$

In the upper layers of the ocean, where temperature and salinity perturbations are weakly correlated, γ is usually set to zero, while in the deep layers it is useful to set it fairly close to 1 (Ricci et al. 2005). From the viewpoint of numerics, introduction of the balanced salinity component is reduced to redefinition of the coefficients α and β in the equation of state:

$$\alpha \longrightarrow \alpha(1+\gamma\theta), \qquad \beta \longrightarrow \beta\sqrt{1-\gamma^2}. \tag{14}$$

In the present report, we describe the numerical implementation of Eq. (7)–(12), which has been derived from the NCOM code (Section 2.1). Since the adjoint of $\mathbf{L}$ is crucial for constraining the background covariance (BEC) and the descent process used in the data assimilation, the code for $\mathbf{L}^{\mathsf{T}}$ has been also constructed (Section 2.2).

1.2 Adjoint of the Balance Constraints and the Background Error Covariance

Partitioning (1) of the state vector implies the following structure for the BEC matrix (assuming $\langle \mathbf{x}_1 \tilde{\mathbf{x}}_2 \rangle = 0$):

$$\mathbf{B} \equiv \langle \mathbf{y}\mathbf{y}^{\mathsf{T}} \rangle = \begin{bmatrix} \langle \mathbf{x}_1 \mathbf{x}_1^{\mathsf{T}} \rangle & \langle \mathbf{x}_1 \mathbf{x}_2^{\mathsf{T}} \rangle \\ \langle \mathbf{x}_2 \mathbf{x}_1^{\mathsf{T}} \rangle & \langle \mathbf{x}_2 \mathbf{x}_2^{\mathsf{T}} \rangle \end{bmatrix} = \begin{bmatrix} \mathbf{B}_1 & \mathbf{B}_1\mathbf{L}^{\mathsf{T}} \\ \mathbf{L}\mathbf{B}_1 & \mathbf{L}\mathbf{B}_1\mathbf{L}^{\mathsf{T}} + \mathbf{B}_2 \end{bmatrix} = \begin{bmatrix} \mathbf{E}_1 & \mathbf{0} \\ \mathbf{L} & \mathbf{E}_2 \end{bmatrix} \begin{bmatrix} \mathbf{B}_1 & \mathbf{0} \\ \mathbf{0} & \mathbf{B}_2 \end{bmatrix} \begin{bmatrix} \mathbf{E}_1 & \mathbf{L}^{\mathsf{T}} \\ \mathbf{0} & \mathbf{E}_2 \end{bmatrix} \tag{15}$$

Here $\mathbf{B}_1 = \langle \mathbf{x}_1 \mathbf{x}_1 \rangle$ and $\mathbf{B}_2 = \langle \tilde{\mathbf{x}}_2 \tilde{\mathbf{x}}_2 \rangle$ are the $M_1 \times M_1$ and $M_2 \times M_2$ BEC matrices of the unbalanced components of $\mathbf{y}$ and $\mathbf{E}_{1,2}$ are the identity matrices of the respective sizes.

In many applications (such as NCODA 3dVar and 4dVar), $\mathbf{B}_{1,2}$ are represented by

$$\mathbf{B}_{1,2} = \mathbf{V}_{1,2}\mathbf{C}_{1,2}\mathbf{V}_{1,2}, \tag{16}$$

where $\mathbf{V}_{1,2}$ are the diagonal rms background error variance matrices of $\mathbf{x}_1$ and $\tilde{\mathbf{x}}_2$, and $\mathbf{C}_{1,2}$ are the respective correlation matrices modeled by the polynomials of the diffusion operator Δ (e.g., Weaver and Courtier 2001; Yaremchuk and Sentchev 2012; Yaremchuk et al. 2013). In particular, the correlation models currently available at NRL have the form:

$$\mathbf{C}_p \simeq [\mathbf{E} - \frac{a^2}{4}\Delta]^{-2}, \qquad \mathbf{C}_e \simeq \exp[\frac{b^2}{2}\Delta], \tag{17}$$

where a and b are the decorrelation radii and Δ is the Laplacian operator. Note that $\mathbf{C}_p$ can be used in both state-space and observation space 3d/4dVar formulations, whereas $\mathbf{C}_p$ is not invertible and, therefore, can be used either in an observation space formulation or in a $\mathbf{B}$-preconditioned state-space approach.

Substitution of (16) into (15) provides the following factorizations of $\mathbf{B}$ and $\mathbf{B}^{-1}$:

$$\mathbf{B}^{-1} = \mathbf{V}^{-1}\mathbf{C}^{-1}\mathbf{V}^{-\mathsf{T}}, \qquad \mathbf{B} = \mathbf{V}\mathbf{C}\mathbf{V}^{\mathsf{T}}, \tag{18}$$

where

$$\mathbf{V} = \begin{bmatrix} \mathbf{E}_1 & \mathbf{0} \\ \mathbf{L} & \mathbf{E}_2 \end{bmatrix} \begin{bmatrix} \mathbf{V}_1 & \mathbf{0} \\ \mathbf{0} & \mathbf{V}_2 \end{bmatrix}, \qquad \mathbf{C} = \begin{bmatrix} \mathbf{C}_1 & \mathbf{0} \\ \mathbf{0} & \mathbf{C}_2 \end{bmatrix}. \tag{19}$$

Furthermore, since

$$\mathbf{V}^{-1} = \begin{bmatrix} \mathbf{V}_1^{-1} & \mathbf{0} \\ \mathbf{0} & \mathbf{V}_2^{-1} \end{bmatrix} \begin{bmatrix} \mathbf{E}_1 & \mathbf{0} \\ -\mathbf{L} & \mathbf{E}_2 \end{bmatrix}, \tag{20}$$

the balanced BEC and its inverse allow explicit symmetric factorization using the square roots of the correlation matrices (17):

$$\mathbf{B}^{-1} = \mathbf{B}^{-\mathsf{T}/2}\mathbf{B}^{-1/2}, \qquad \mathbf{B} = \mathbf{B}^{1/2}\mathbf{B}^{\mathsf{T}/2}, \qquad \text{with} \quad \mathbf{B}^{1/2} = \mathbf{V}\mathbf{C}^{1/2}, \tag{21}$$

which is an important property ensuring the computational efficiency of many data assimilation algorithms. Expressions for the balanced BEC and its inverse have the form:

$$\mathbf{B}^{-1} = \begin{bmatrix} \mathbf{B}_1^{-1} + \mathbf{L}^{\mathsf{T}}\mathbf{B}_2^{-1}\mathbf{L} & -\mathbf{L}^{\mathsf{T}}\mathbf{B}_2^{-1} \\ -\mathbf{B}_2^{-1}\mathbf{L} & \mathbf{B}_2^{-1} \end{bmatrix}, \qquad \mathbf{B} = \begin{bmatrix} \mathbf{B}_1 & \mathbf{B}_1\mathbf{L}^{\mathsf{T}} \\ \mathbf{L}\mathbf{B}_1 & \mathbf{L}\mathbf{B}_1^{-1}\mathbf{L}^{\mathsf{T}} + \mathbf{B}_2 \end{bmatrix}, \tag{22}$$

which explicitly shows the necessity of having the adjoint code ($\mathbf{L}^{\mathsf{T}}$) for operations with the balanced BEC and its inverse.

Finally, the matrix $\mathbf{G} = \mathbf{V}\mathbf{V}^{\mathsf{T}}$ can be effectively used as a natural metric in the space of cost function gradients. The associated geometry inhibits descent in the unbalanced directions and, therefore, has the potential to make the 3d/4dVar optimization processes more efficient in recovering balanced corrections to the background state.

2. CODE DESCRIPTION

The algorithms that comprise the NCOM computational kernel are described in detail by Martin (2000), with some of the more recent additions described by Morey et al. (2003) and Barron et al. (2006). The vertical mixing models that are used in NCOM are the Mellor-Yamada level 2 (Mellor and Yamada 1974) and level $2\frac{1}{2}$ (Mellor and Yamada 1982) turbulence closure schemes. The equation of state used is that of Mellor (1991). There are options for several advection schemes, of which the most commonly used is third-order upwind (Holland et al. 1998), which implicitly includes biharmonic diffusion.

The balance operator is written as a subroutine, `ncom_balanced`, which is called to compute the sea-surface height (SSH) and velocity perturbations from the input temperature and salinity perturbations. As noted in the previous section, two methods of computing the SSH perturbations are provided: (a) the solution of a elliptic equation formed from the horizontal divergence of the linearized, depth-integrated, barotropic and baroclinic pressure gradient terms of the horizontal momentum equations and the depth-integrated continuity equation (8), and (b) a dynamic height calculation using a specified level of no motion (Eq. (11)).

2.1 Dynamic Height Calculation for SSH Perturbations

Subroutine `denp_lin` is called to compute density perturbations ρ' from temperature and salinity perturbations, T' and S', respectively, using the linearized equation of state

$$\rho' = \alpha(\boldsymbol{x}, z)T' + \beta(\boldsymbol{x}, z)S'. \tag{23}$$

The equation of state is linearized around reference values of temperature and salinity using coefficients of thermal and salinity expansion, α and β, respectively.

Subroutine `bpg_term` is called to compute baroclinic pressure gradient perturbation terms from the density perturbations ρ'. These are computed using the same numerics as used in NCOM (Martin 2000), i.e., on the sigma coordinate part of the grid, the baroclinic pressure gradient perturbation in the x-direction is calculated for the kth layer as

$$\frac{1}{\rho_o}\frac{\partial p'}{\partial x}|_k = \frac{1}{\rho_o}\frac{\partial p'}{\partial x}|_{k-1} + \frac{g}{\rho_o \Delta x^u}(\frac{1}{4}D^u(\Delta\sigma_{k-1}+\Delta\sigma_k)\delta_x(\rho'_{k-1}+\rho'_k) - \frac{1}{2}(\sigma_{k-1}+\sigma_k)(\delta_x D)(\delta_z\overline{\rho'}^x)), \tag{24}$$

and on the z-level part of the grid, the baroclinic pressure gradient perturbation is calculated as

$$\frac{1}{\rho_o}\frac{\partial p'}{\partial x}|_k = \frac{1}{\rho_o}\frac{\partial p'}{\partial x}|_{k-1} + \frac{g}{\rho_o \Delta x^u}\frac{1}{2}(\Delta z_{k-1}\delta_x\rho'_{k-1} + \Delta z_k \delta_x \rho'_k), \tag{25}$$

where Δx^u is the local grid spacing in the x direction at a u point, $\Delta\sigma_k$ is the fractional thickness of sigma layer k at a T point, Δz_k is the layer thickness on the z-level part of the grid, δ_x is the differential operator in the x direction, δ_z is the differential operator in the vertical direction, D^u is the total depth of the sigma part of the grid at a u point, D is the total depth of the sigma part of the grid at a T point, and the overbar indicates a horizontal average in the specified direction. The baroclinic pressure gradient perturbation in the y-direction is calculated analogously.

Subroutine `dyn_ht` is called to compute SSH perturbations ζ' from the density perturbations ρ' using a dynamic height calculation and an assumed level of no motion, i.e.,

$$\zeta' = -\frac{1}{\rho_o}\sum \rho'_k \Delta z_k, \tag{26}$$

where the sum is computed from the assumed level of no motion to the surface. Note that the layer thickness for layers on the sigma part of the grid is computed as $\Delta z_k = D\Delta\sigma_k$.

Subroutine `vel_geo` is called to compute velocity perturbations u', v' from the baroclinic pressure gradient and SSH perturbations assuming geostrophy, i.e.,

$$u' = \overline{-\frac{1}{\overline{f}^y}\frac{1}{\rho_o}\frac{\partial p'}{\partial y} - \frac{g}{\overline{f}^y}\frac{\delta_y\zeta'}{\Delta y^v}}^{xy}, \tag{27}$$

$$v' = \overline{\frac{1}{\overline{f}^x}\frac{1}{\rho_o}\frac{\partial p'}{\partial x} + \frac{g}{\overline{f}^x}\frac{\delta_x\zeta'}{\Delta x^u}}^{xy}, \tag{28}$$

where f is the local Coriolis parameter, Δy^v is the local grid spacing in the y direction at a v point, and the overbars indicates horizontal averaging in the specified direction(s).

2.2 Solution of an Elliptic Equation for the SSH Perturbations

The alternate method for computing the SSH perturbations is to solve Eq. (8), an elliptic equation for the SSH perturbations. The finite difference form of this equation that is used (which is similar to the form used within NCOM to update the SSH) is

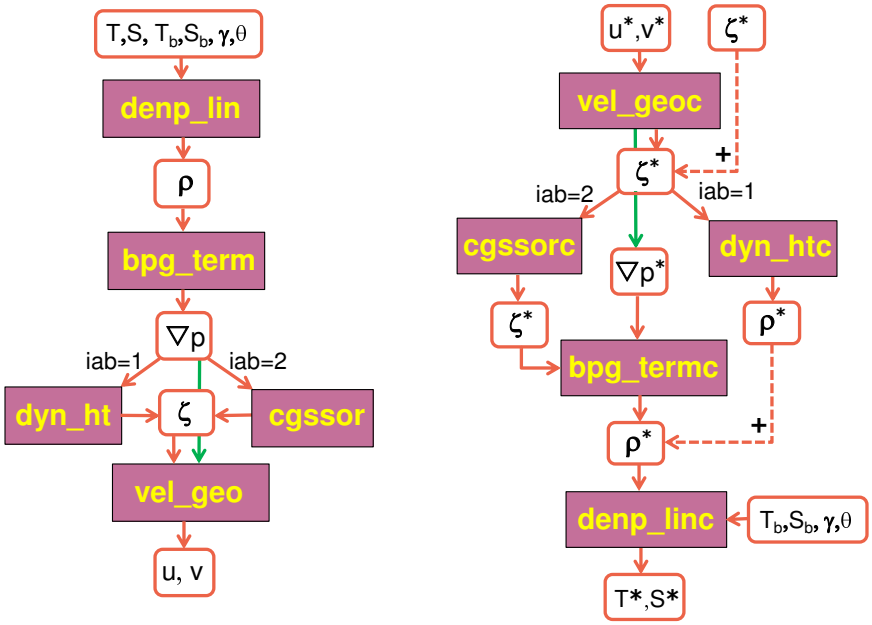

Fig. 1 — Flow chart for the balance operator code (left), and for the adjoint code for the balance operator (right).

$$\delta_x\left(\frac{\Delta y^u g H^u}{\Delta x^u}\delta_x\zeta'\right)+\delta_y\left(\frac{\Delta x^v g H^v}{\Delta y^v}\delta_y\zeta'\right)=-\delta_x\left(\Delta y^u\sum\frac{\Delta z_k^u}{\rho_o}\frac{\partial p'}{\partial x}|_k\right)-\delta_y\left(\Delta x^v\sum\frac{\Delta z_k^v}{\rho_o}\frac{\partial p'}{\partial y}|_k\right) \qquad (29)$$

where H^u is the total depth at a u point, H^v is the total depth at a v point, and the sums are taken in the vertical over the whole depth of the water column. This equation is solved for the SSH perturbations using a pre-conditioned, conjugate-gradient method. Note that, relative to Eq. (8), in forming Eq. (29), the x- and y component equations were multiplied by the grid-cell area before taking the horizontal divergence so that the coefficients input to the elliptic solver would be symmetric.

2.3 Direct Code

The flow chart on the left side of Figure 1 shows the structure of the code for the balance operator realized in subroutine `ncom_balanced`. The NCOM grid parameters are passed into `ncom_balanced` in the subroutine argument list to improve the flexibility of the code in accommodating nested grids. The subroutine sequentially solves the system of Eq. (7)-(11) discretized in a manner consistent with the NCOM formulation.

Specifically, the constituents of `ncom_balanced` perform the following operations:

- `denp_lin`: computes density perturbations via Eq. (7),(23)
  . calls `ce_mel3` to compute expansion coefficients α and β using γ and θ via Eq. (14).
- `bpg_term` - computes baroclinic pressure gradients via Eq. (9),(24)–(25).

- `cgssor`: solves for SSH using Eq. (8),(29)
  . calls `minmax1`
- `dyn_ht`: computes SSH using Eq. (11),(26)

- `vel_geo`: computes horizontal velocities using Eq. (10),(27)–(28)
  . calls `avev` and `aveu` to interpolate between the u and v-grids.

Switching between the modes is made by changing the parameter `iab`, i.e., `iab=1` invokes the b-mode and `iab=2` invokes the a-mode.

2.4 Adjoint Code

The flow chart on the right side of Figure 1 shows the structure of the code for the adjoint of the balance operator realized in subroutine `ncom_balanced`. Similar to `ncom_balanced`, the grid parameters are passed into `ncom_balancea` within the subroutine argument list to improve the flexibility of the code in accommodating nested grids. The subroutine sequentially solves the adjoints of Eq. (7)-(11) in the reverse order.

Specifically, the components of `ncom_balancea` perform the following operations:

- `vel_geoc`: computes the adjoint of the velocity perturbation Eq. (10),(27)–(28)
  . calls `avevc, aveuc`, the adjoints of the interpolation between the u and v grids.
- `cgssorc`: solves the adjoint of Eq. (8),(29)
  . calls `minmax1`.
- `dyn_htc`: computes the contribution to the adjoint density perturbation Eq. (11),(26).
- `bpg_termc`: computes the contribution to the adjoint density from the adjoint pressure gradients Eq. (9),(24)–(25).
- `denp_linc`: computes the adjoint temperature and salinity Eq. (7),(23).
  . calls `ce_mel3` to compute expansion coefficients α and β using γ and θ Eq. (14).

3. TESTING

3.1 NCOM Configuration

The model was configured at 3-km resolution on an 85×294 horizontal grid, with 32 levels in the vertical. The top 22 σ levels follow the bathymetry from the surface to a maximum depth of 291 m, and 10 fixed-depth levels are used below 291 m. Initial and open boundary conditions for the SSH ζ, temperature T, salinity S, and horizontal velocities u, v were obtained from Global NCOM, which was run operationally at the Naval Oceanographic Office (Barron et al. 2004). Tidal forcing was not used in this application. The Adriatic model was forced by river runoff and by atmospheric fields derived from the 8-km horizontal resolution, regional ALADIN atmospheric model (Ivatek-Sahdan and Tudor 2004).

In the described numerical experiments, the state vector $\mathbf{y}$ comprised all the grid point values of ζ, T, S, u, and v. With the given 3-dimensional grid and bathymetry, the state vector has M=1,493,570 components. The dimension M_2 of the balanced constituent was equal to 743,526

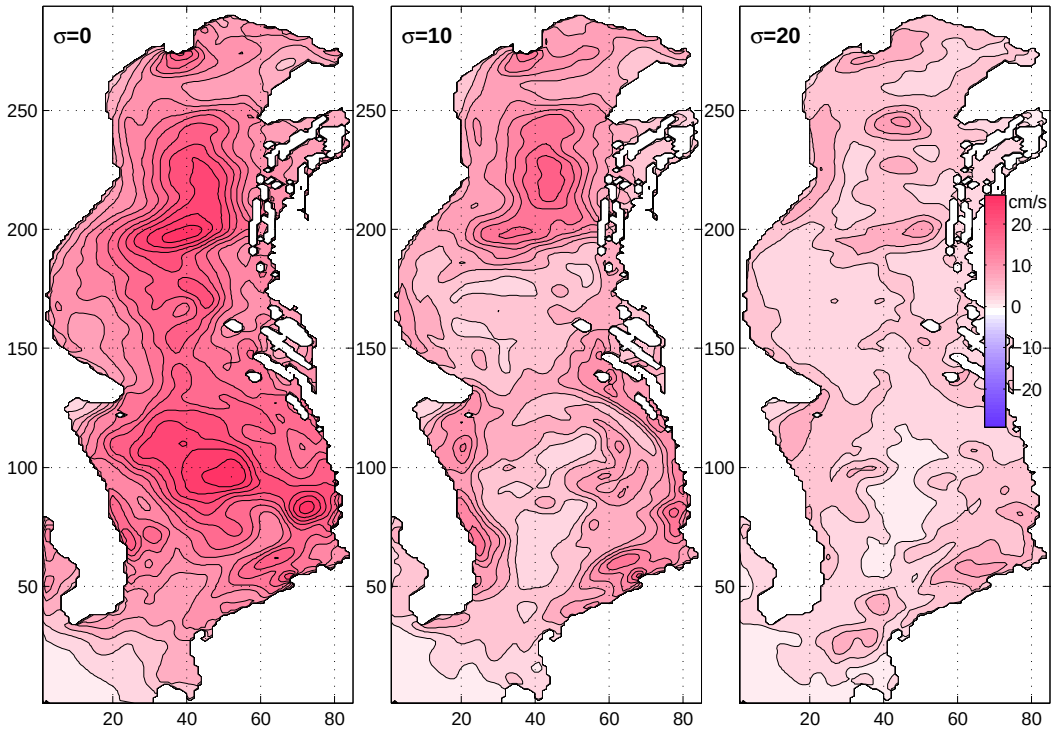

Fig. 2 — Maps of the diagonal elements of $\mathbf{V}_2$ corresponding to the unbalanced rms error variance of the horizontal velocity at three σ-levels.

(the number of $\vec{\boldsymbol{u}}, \zeta$ grid points). The background values of $\mathbf{y}(t)$ were taken from the NCOM simulation described by Martin et al. (2009) and then adjusted to suppress temperature and salinity biases during the assimilation time interval (from 0.00 UTC on 08/14 to 0.00 UTC on 08/29/2006). After the adjustment, the horizontally- and temporally-averaged misfits between the background solution and the T and S observations did not exceed 0.02°C and 0.005 psu, respectively.

3.2 Balanced and Unbalanced Perturbations

The relative magnitude of the ageostrophic motions in the model solution was assessed by the non-dimensional parameter

$$\kappa_z(t) = R\frac{\overline{|\mathrm{div}(\vec{\boldsymbol{u}})|}^{xyz}}{\overline{|\vec{\boldsymbol{u}}_b|}^{xyz}}, \tag{30}$$

where $\vec{\boldsymbol{u}}(\boldsymbol{x}, z, t)$ is the horizontal velocity of the solution, b denotes the background or reference solution, the overbar indicates 3d averaging in the depth interval between the surface and depth z, and $R = 9$ km is the Rossby radius of deformation (Cushman-Rosin and Korotenko 2007). The definition (30) does not account for the divergence of the geostrophic currents, which is negligible in the considered regional application.

To assess the impact of the increments generated by the data assimilation procedure, we perturbed the initial conditions of the background solution. The 3d structure for the simulated increments were generated as follows. First, we defined the background error correlation model $\mathbf{C}_p$ using Eq. (17). Second, 300 eigenvectors corresponding to the 300 largest eigenvalues of $\mathbf{B}$ were computed,

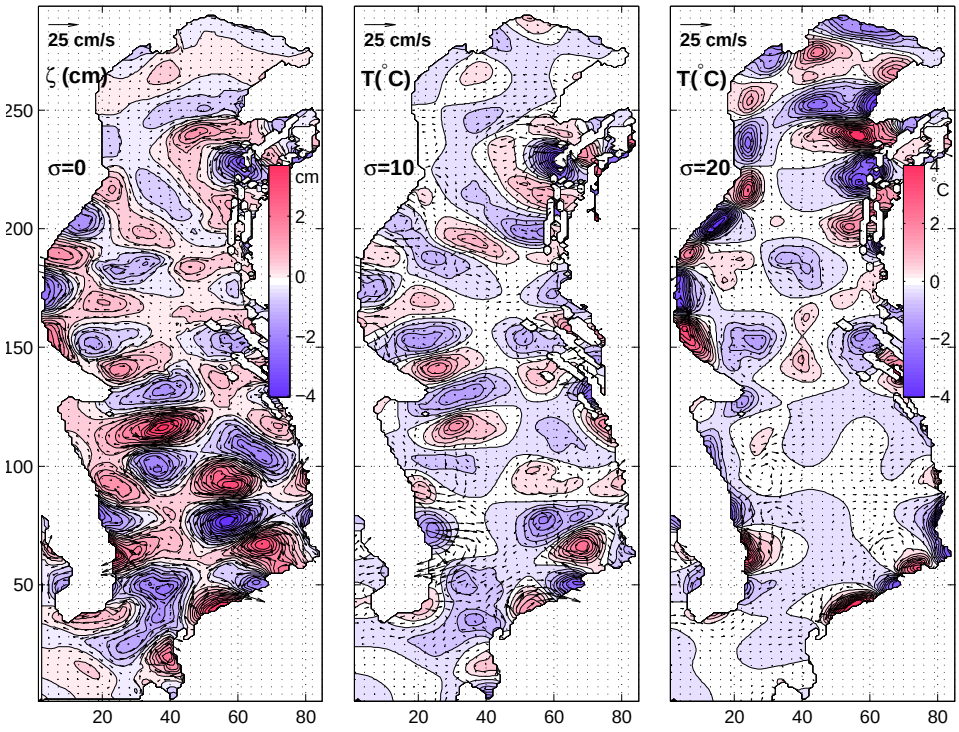

Fig. 3 — Maps of SSH, temperature (color) and velocity perturbations on three σ-levels constrained by the $\mathbf{L}_a$ operator

solving the generalized eigenvalue problem $\mathbf{B}^{-1}\mathbf{e}_l = \lambda_l \mathbf{G}^{-1}\mathbf{e}_l$ and the last (l =300) eigenvector $\mathbf{e}$ was elected to compute the perturbations.

The actual perturbations $\delta\boldsymbol{x}$ of the initial conditions were defined by rescaling the eigenvector by a factor ε whose magnitude was chosen in such a way that the σ-grid root-mean-square value of the temperature perturbation field was equal to 0.8°C.

$$\delta\boldsymbol{x} = \varepsilon \mathbf{e}_{300}. \tag{31}$$

The diagonal elements of $\mathbf{V}_1$ and $\mathbf{V}_2$ in Eq. (19) were obtained as time-averaged rms variances of the background fields. Since the diagonal of $\mathbf{V}_2$ represents the ageostrophic (unbalanced) constituents of the velocity and SSH fields, the respective background rms variances were multiplied by the mean value of κ (Section 3.3), which characterizes the level of the ageostrophic motions in the background solution.

Three types of perturbations were tested:

- balanced perturbations (Fig. 3) computed with the integral continuity constraint (operator $\mathbf{L}_a$ in Eq. (19) defined by Eq. (7)–(10));
- balanced perturbations (Fig. 4) computed with the assumption of zero pressure anomalies at the bottom (operator $\mathbf{L}_b$ defined by Eq. (7), (8)–(11))
- unbalanced perturbations computed with $\mathbf{L} = 0$ in Eq. (19).

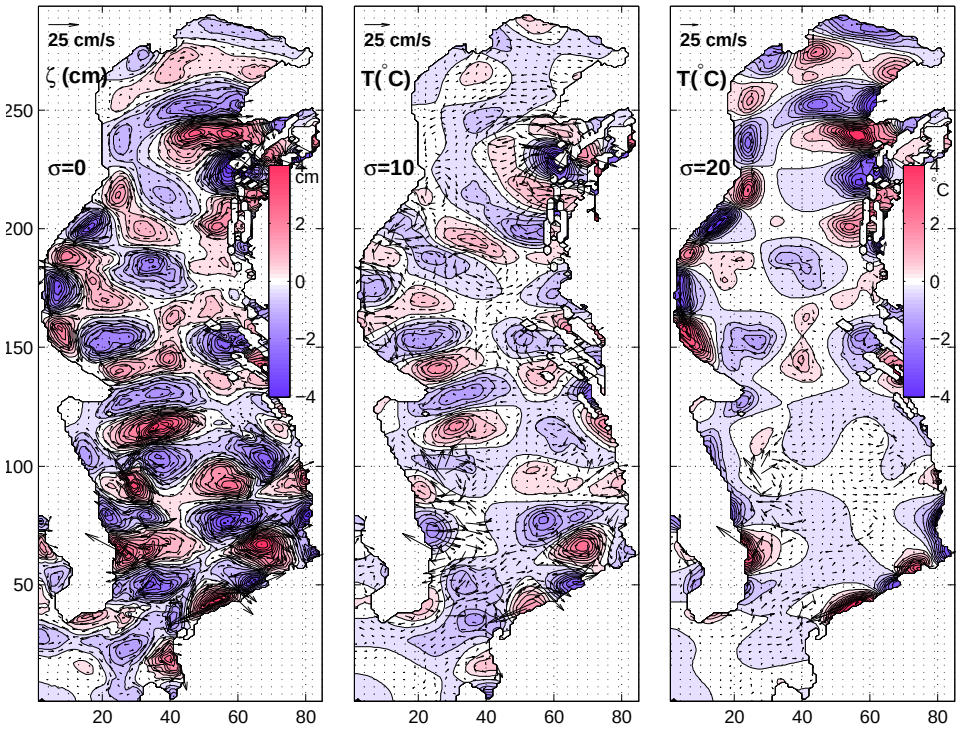

Fig. 4 — Maps of SSH, temperature (color) and velocity perturbations on three σ-levels constrained by the $\mathbf{L}_b$ operator.

3.3 Results

The background run of the model was executed from August 9 to August 24, 2006. Since the Adriatic Sea is mostly shallow (depths less than 280 m occupy 78% of the area), the value of κ was computed by averaging over the upper 22 σ layers. The mean value of κ during the background integration period was 0.38, indicating the presence of a significant ageostrophic component, which was primarily associated with inertial oscillations and upper-layer Ekman dynamics.

The time evolution of the difference between the values for κ for the perturbed and background solutions is shown in Fig. 5. As can be seen in Fig. 5, κ grows by a factor of 1.6 (from 0.4 to 0.64) after the perturbation of the model on August 9 with unbalanced perturbations, whereas κ experiences only modest growth for the b-balanced (32%) and a-balanced (19%) perturbations.

The advantage of lower ageostrophic shocks provided by the a-type perturbations comes at an additional computational cost: application of the a-type balance operator $\mathbf{L}_a$ consumes 5.5 times more CPU time than application of $\mathbf{L}_b$ (0.171 sec against 0.031 sec on a single 2.3 Ghz processor). For the tested state vector (M =1,493,570), these CPU requirements can, however, be considered to be negligible compared to the CPU time required by the model integration for 1 day (60 sec on single processor). For that reason, the balance operator and its adjoint can be considered to be relatively computationally inexpensive components of an assimilation cycle.

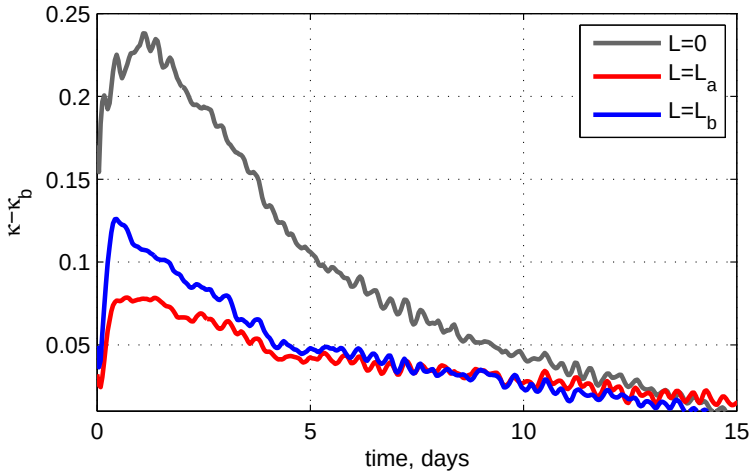

Fig. 5 — Time evolution of the difference in the values of κ between the background solution and the three types of perturbed solutions.

4. SUMMARY

The balance operator code that has been developed can be used in NRL data assimilation systems for the purpose of constraining the innovations to a "slow" (hydrostatically and geostrophically balanced) manifold. This will allow efficient extraction of the most persistent modes from the incoming data. More importantly, the balance operator approach will provide more flexibility in constraining the background covariances to the user-defined subspaces fully consistent with the numerics of the parent model. This will enable a flexible, modular approach to the construction of the covariance operators and require code development for the dynamical constraints defined by the user together with their adjoints (a relatively inexpensive procedure compared to the modification of the existing NCODA system, where the balance constraints are hard-wired in the correlation operator code). The balance operator could be used in upgrading NCODA 3d- and 4dVar (Ngodock and Carrier 2014) data assimilation systems and could be also useful in similar atmospheric applications (Xu and Rosmond 2004; Rosmond and Xu 2006).

The balance operator code presented in this report can be further developed to include the parameterization of equatorial dynamics, non-linear terms on the right-hand side of the elliptic equation for the SSH perturbations, and MPI parallelization.

5. ACKNOWLEDGMENTS

This work was funded through the 6.1 NRL Core Projects "Adjoint-free 4dVar for Navy Ocean Models" (Program Element Number 61153N) and "Coupled Ocean-Atmosphere Variational Assimilation" (Program Element Number 62435N).

6. REFERENCES

Barron, C.N., A.B. Kara, H.E. Hurlburt, C. Rowley, and L.F. Smedstad (2004). "Sea Surface Height Predictions from the Global Navy Coastal Ocean Model (NCOM) During 1998–2001," *J. Atmos. Oceanic Technol.* **21**(12), 1876–1894.

Barron, C. N., A. B. Kara, P. J. Martin, R. C. Rhodes, and L. F. Smedstad, (2006). "Formulation, implementation and examination of vertical coordinate choices in the global Navy Coastal Ocean Model (NCOM)", *Ocean Modell.*, **11**, 347-375, doi:10.1016/j.ocemod.2005.01.004

Cushman-Roisin, B., and K. A. Korotenko, (2007). "Mesoscale-resolving simulations of summer and winter bora events in the Adriatic Sea", *J. Geophys. Res.*, **112**, C11S91.

Cullen, M. J. P. (2003). "Four-dimensional variational data assimilation: A new formulation of the background-error covariance matrix based on a potential-vorticity representation". *Q. J. R. Meteorol. Soc.*, **129**, 2777-2796.

Derber, J. and F. Bouttier, (1999). "A reformulation of the background error covariance in the ECMWF global data assimilation system", *Tellus*, **51A**,195–221.

Ivatek-Sahdan, S., and M. Tudor, (2004) "Use of high-resolution dynamical adaptation in operational suite and research studies", *Meteorol. Z.*, **13**, 1–10.

Holland, W.R., J.C. Chow, and F.O. Bryan (1998). "Application of a third-order-upwind scheme in the NCAR Ocean Model", *J. Clim.*, **11**, 1487–1493.

Martin, P.J. (2000). "A Description of the Navy Coastal Ocean Model Version 1.0," NRL Report NRL/FR/7322–00-9962, Naval Research Laboratory, SSC, MS 39529, 42 pp.

Martin, P. J., J. W. Book, D. M. Burrage, C. D. Rowley, and M. Tudor (2009). "Comparison of model-simulated and observed currents in the central Adriatic during DART", *J. Geophys. Res.*, **114**, C01S05, doi:10.1029/2008JC004842.

Mellor, G. L., (1991). "An equation of state for numerical models of oceans and estuaries", *J. Atmos. Oceanic Technol.*, **8**, 609-611.

Mellor, G.L. and T. Yamada (1974). "A Hierarchy of Turbulence Closure Models for Planetary Boundary Layers," *J. Atmos. Sci.* **31**, 1791–1806.

Mellor, G.L. and T. Yamada (1982). "Development of a Turbulence Closure Model for Geophysical Fluid Problems," *Geophys. and Space Phys.* **20**, 851–875.

Mirouze, I., and A. Weaver, (2010). "Representation of correlation functions in variational data assimilation using an implicit diffusion operator", *Quart. J. Roy. Meteorol. Soc.*, **136**, 1421-1443.

Morey, S. L., P. J. Martin, J. J. OBrien, A. A. Wallcraft, and J. Zavala-Hidalgo, (2003). Export pathways for river discharged fresh water in the northern Gulf of Mexico, *J. Geophys. Res.*, **108**(C10), 3303, doi:10.1029/2002JC001674.

Ngodock, H., and M. Carrier, (2014). "A 4dVar system for the Navy Coastal Ocean Model. Part I: system description and assimilation of synthetic observations in Monterey Bay", *Mon. Wea. Review*, **142**(6), 2085–2107.

Ricci, S., Weaver, A. T., Vialard, J. and Rogel, P., (2005). "Incorporating temperaturesalinity constraints in the background error covariance of variational ocean data assimilation". *Mon. Weather Rev.*, **133**, 317-338

Rosmond, T., and L. Xu, (2006). "Development of the NAVDAS-AR: non-linear formulation and outer loop tests", *Tellus*, **58A**, 45–58.

Weaver, A. T., and P. Courtier, (2001). "Correlation modelling on a sphere using a generalized diffusion equation" *Q. J. R. Meteorol. Soc.* **127**, 1815-1846.

Weaver, A. T., C. Deltel, E. Machu, S. Ricci and N. Daget, (2005). "A multi-variate balance operator for variational data assimilation", *Q. J. R. Meteorol. Soc*, **131**, 3605–3625.

Xu, L., and T. Rosmond, (2004). "Formulation of the NRL Atmospheric Variational Data Assimilation System - Accelerated Representer (NAVDAS-AR)", NRL/MR/7532-36, *Naval Research Laboratory Report*, 28 pp.

Yaremchuk, M., and A. Sentchev, (2012). "Multi-scale correlation functions associated with polynomials of the diffusion operator", *Q. J. Roy. Met. Soc.*, **138**, 1948–1953.

Yaremchuk, M., M. Carrier, S. Smith, and G. Jacobs, (2013). "Background error correlation modeling with diffusion operators". In: *Data Assimilation for Atmospheric, Oceanic and Hydrological Applications*, S. K. Park and L. Xu, Eds., Vol. 2, Springer, 177–203.